

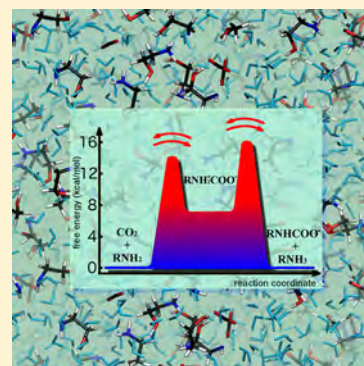
Capture and Release of CO₂ in Monoethanolamine Aqueous Solutions: New Insights from First-Principles Reaction Dynamics

Changru Ma, Fabio Pietrucci, and Wanda Andreoni*

Institut de Théorie des Phénomènes Physiques, Ecole Polytechnique Fédérale de Lausanne, Lausanne, Switzerland

S Supporting Information

ABSTRACT: Aqueous monoethanolamine (MEA) solution is commonly used for post-combustion carbon capture via chemical absorption. Extensive research has been carried out to characterize both uptake and release of carbon dioxide (CO₂), with the aim of improving process performance. However, an intensive research is still needed on fundamental aspects of the cyclic process at the microscopic level and a quantitative assessment. We present several *ab initio* simulations of MEA solutions at a concentration of 30 wt %—the current standard in the industry—and study the dynamics of key multistep chemical reactions, using the metadynamics technique. Pathways for the entire cycle are investigated and characterized in terms of related free-energy and enthalpy barriers, and of the accompanying variations in both structural and electronic properties. The results of this study lead us to propose, among competing processes, an unforeseen scenario in which the zwitterion acts as an intermediate not only of CO₂ uptake, in the form of carbamate, but also of its release. Rate-limiting steps are the formation of the zwitterion for the former and MEAH⁺ deprotonation for the latter. Water is shown to play a multifaceted role, which is crucial in determining the development and the energetics of each step of the reactions. The level of comprehension here achieved for MEA should help defining a strategy for solvent optimization.



1. INTRODUCTION

Post-combustion carbon capture mainly employs solvent wet scrubbing, in a cyclic process that implies both uptake and release of carbon dioxide in chemical absorbents.^{1,2} Alkanolamine aqueous solutions are most frequent in industrial applications and primarily monoethanolamine (MEA) at a concentration of 30 wt %. MEA solutions exhibit several unique advantages, e.g., high reactivity with CO₂, relatively low solvent cost and special ease of reclamation,³ but are known to be corrosive⁴ and to require high regeneration energy.⁵ This situation has led to extensive empirical search for alternatives⁶ but also motivates research at more fundamental level, aiming at a deeper understanding of the chemistry of MEA solutions and especially of the processes following CO₂ solvation. Several issues have been clarified over the years but knowledge at the microscopic level is still incomplete and quantitative characterization of the single reaction steps is essentially missing.

We recall that the overall reaction of CO₂ with aqueous MEA can be expressed as



where R = CH₂CH₂OH.

After Caplow's seminal work⁷ on dilute solutions, it has been generally accepted that the most probable early event in the capture from aqueous MEA is the formation of a zwitterion. This hypothesis was found to be consistent with most analyses of the kinetics of the reactions (see, e.g., refs 8–10). Still, the zwitterion eludes direct observation. Moreover, there is

experimental evidence that carbamate is the prevailing product of the CO₂ interaction with the MEA solution¹¹—by far, dominant over bicarbonate—and that release requires too high temperatures. In summary, the two steps implied in the zwitterion mechanism can be written as



where RNH₂⁺COO⁻ and RNHCOO⁻ represent the zwitterion and the carbamate, respectively, and B is any of the bases present in the solution, namely, either an amine or a water molecule or a hydroxide ion.

Fundamental questions arise that urgently need to be answered: Why is zwitterion formation slower than dissociation? What makes CO₂ release from carbamate “slow”? How do the characteristics of the solution influence these reactions? In particular, what is the role of water? What is the effect of amine concentration or, in other words, to what extent do neighboring amines participate in the different stages of the cyclic process? The difficulty to answer any of such questions with targeted experiments is a severe obstacle for the application of rational design to the search of alternative solvents, and calls for the aid of an approach based on robust theoretical and computational methods. Our work aims at establishing such a protocol, based

Received: January 18, 2015

Published: May 19, 2015

on state-of-the-art simulations and provide an answer to the above questions.

Indeed, beyond kinetic models of diverse levels of sophistication, computational attempts to characterize the reactions accompanying CO₂ wet capture are still only a few and limited in the information they can provide. Several results of the previous calculations^{12–20} are recalled here, not only for their relevance to the issues we tackle but also as a basis for comparison of the present work. To this aim, more details are also reported in section 2.

Pioneering work by da Silva, Svendsen, and collaborators (e.g., in refs 12–14 and ref 21) used classical molecular dynamics (MD) or Monte Carlo simulations, also combined with molecular quantum-mechanical calculations. These have led to a broad characterization of the relevant amine solutions and have given hints into the complicated and various problems involved in the simulation of their interaction with CO₂. Regarding the chemical reactions of interest here, the formation of the carbamate¹² is simulated through a series of geometry optimizations for structures containing a few explicit molecular units—CO₂, one or two MEAs, and one or three explicit water molecules—in the gas phase, treated at the Hartree–Fock level. Energy differences are then corrected for the presence of water, represented by a continuum solvation model. These calculations led the authors to propose that the progressive approach of CO₂ to MEA simultaneously drives a “gradual proton transfer” to a water molecule acting as the base. In this scenario, it is argued that the origin of the reaction barrier for the carbamate formation must be found in the attempt of CO₂ to displace water molecules in the solvation shell of “the amine groups”. On the other hand, the authors suggest that the two-step mechanism (eqs 2) is not excluded for amines in general, although the zwitterion must be understood as a transient, rather than an intermediate of the reaction.

A similar protocol, namely, a series of geometry optimizations on a prescribed pathway—aided by a transition-state search—and a combined quantum-classical scheme, has been adopted in most of the following studies. These differ in the choice of the set of molecules to be treated quantum-mechanically as well as in the selection of the specific quantum method and of the continuum solvation model representing water (see section 2).

In ref 15, the formation of both carbamic acid (I) and carbamate (II) from the binding of a CO₂ molecule to a MEA, is considered in the simultaneous presence of one water molecule and an additional MEA. At variance with the work by da Silva et al., here, the quantum description of the molecules, still in the gas phase, was obtained within a scheme combining density functional theory (DFT) for geometry optimization and energy corrections for electron correlation. In both processes, the key role of the additional MEA was emphasized, either as “direct” catalyst in I or as proton acceptor in II, whereas the water molecule was only a passive spectator of the reactions but lowered the activation energy. The accuracy of the computations did not allow one to identify a preference for one mechanism or the other. However, in view of the experimental knowledge that the order of each sorption process in the uptake reaction is one for MEA, the formation of carbamic acid was argued to be more probable.

Other approaches concern carbamate formation through the zwitterion mechanism (eqs 2). In ref 16, the *ab initio* framework used for the interacting molecules is that of DFT, water is represented by a polarizable solvation model, and its

effects on the structure of the molecular complexes are taken into account. Two cases are considered: with CO₂ and MEA accompanied by either an additional MEA or a water molecule. In both, the complex with a zwitterion is found to be more stable than the separated entities. However, after deprotonation, the system carbamate plus protonated MEA turns out to be energetically favored, with respect to carbamate plus hydronium, thus leading the authors to propose that “MEA is suitable as a base but H₂O is not”. However, they also suggest the possibility of a very fast proton transfer through an agent water molecule.

In ref 17, the formation of the zwitterion and the proton transfer to another MEA were studied in two ways. First, in analogy to ref 15, a procedure was followed in which DFT geometry relaxation of the molecular structures—interacting with the implicit solvent—is augmented by single-point coupled-cluster calculations. CO₂ binding to MEA was found to imply a ~10 kcal/mol barrier, whereas zwitterion deprotonation was spontaneous. Subsequently, these predictions were confirmed by Born–Oppenheimer MD and mean-force potential calculations, with the reacting molecules embedded in an ensemble of water molecules interacting via a classical force field. Regarding the estimate of the entropy contribution to free-energy differences, this was reduced to the change pertaining to the reacting molecules in passing from the gas-phase to the interacting complexes in either the reactant or the product systems. We also remark that the mediating action of water is not contemplated in this study.

In ref 18, both steps in eqs 2 are considered with an additional amine providing the only base for proton abstraction. With the protocol outlined above, both reactions are predicted to be barrierless. This result is further confirmed for zwitterion deprotonation in an ultrashort run of DFT-based MD of a model meant to represent the 30 wt % solution. It consists of a very small periodically repeated cell with one MEA zwitterion, one MEA and a small number of water molecules. The reaction is very fast: starting from a configuration of the two MEAs, they “reorient” within 0.5 ps. Then, proton transfer from one to the other happens—without the intervention of a water molecule—in only 0.6 ps, after overcoming a potential barrier of only 1.3 kcal/mol.

More recent DFT-MD simulations²⁰ of a dilute solution support a barrierless proton transfer from the zwitterion to water for several different amines. In the case of MEA, a small periodically repeated cell was adopted as model corresponding to a 5.4 wt % solution. Deprotonation of the zwitterion was observed to take place “instantly” via a Zundel-ion transient. This especially rapid transfer was commented by the authors as probably being due to the “beneficial local water structure”.

We have recently investigated the dissociation of the zwitterion in dilute (3 wt %) MEA solutions,¹⁹ via either deprotonation or CO₂ loss. Our model consisted of periodically repeated cells of suitable size for the assessment of the solvent effects (122 molecules). The method of choice was DFT (Car–Parrinello²²) molecular dynamics, empowered by the metadynamics (MTD) technique²³ for the enhancement of configuration sampling. Carbamate formation via zwitterion deprotonation turned out to be characterized by a sizable free-energy barrier (7–9 kcal/mol), in disagreement with ref 20. CO₂ release was also found to be activated and to involve free-energy barriers of comparable values. These results were shown to be independent of the method (MTD or umbrella sampling) and of the DFT functional considered (BLYP-D2 or PBE-D2).

Moreover, the specific role of water molecules was identified and found to be crucial for the development of both reactions.

In this paper, we extend this study to simulate the more complex reactions taking place in aqueous MEA solutions at a concentration of 30 wt %, namely, the one employed in industrial processes. We make use of periodically repeated cells of unprecedented size to allow for an understanding the solute–solvent interaction at the nanometer scale. We remark also that, in contrast with most of the calculations mentioned above, no constraint is applied in our protocol, such as to guide the reaction along a given pathway, namely neither the reactant nor the product are set up in prearranged configurations. Indeed, MTD simulations provide useful characterization of each process, in that they reveal the reaction paths and can be used to reconstruct the free-energy surface in the space of the collective variables (CV) chosen as reaction coordinates.

The results of 11 distinct and independent simulations will be discussed, corresponding to the cyclic reactions in eqs 2. They refer to several samples that differ either in size or in the initial configurations of the reactants or in the temperature (300 and 400 K). We recall that, in a previous publication,²⁴ we have examined the equilibrium structures of the aqueous solutions with solvated CO₂ (reactant) and with carbamate (product) for some of these samples and others at a different temperature. In this way, we were able to interpret experimental data revealing the variation of structural characteristics and vibrational spectra of the solution induced by the capture of CO₂. In the following, our results in ref 19 will be recalled and treated as our reference for the understanding of the effects of amine concentration on those specific reactions.

2. METHODS

2.1. Our Simulations and System Setup. We perform DFT (Car–Parrinello²²) molecular dynamics on periodically repeated atomistic models. Our calculations use the BLYP-D2²⁵ approximation for the exchange–correlation functional, namely, a gradient-corrected (GGA) functional including long-range dispersion corrections, and the (norm-conserving) pseudo-potential²⁶ plane-wave scheme as implemented in the CPMD code.²⁷

Several tests of the exchange–correlation functional have been performed and reported in our previous publications: in the Supporting Information for ref 24, calculations of the molecular structures of MEA and carbamate conformers were compared, using different functionals (GGA with Grimme corrections (BLYP-D2, PBE-D2²⁸) and the hybrid B3LYP²⁹); in ref 19, the CO₂ reactions with MEA were studied in a dilute aqueous solution using both the BLYP-D2 and the PBE-D2 functionals. Here, further calculations are presented in the Table S1 in the Supporting Information (SI) on the MEA dimer in the gas phase, performed within DFT in the PBE, BLYP, BLYP-D2, and B3LYP approximations as well as in the second-order Møller–Plesset (MP2) approach. The BLYP-D2 functional that we have chosen for the simulation of the solutions with an amine concentration of 30 wt % is the one giving the best comparison with MP2.

Our simulations refer to five samples that differ for the size and/or the temperature and/or the conformer of the zwitterion and the carbamate. We denote them as L1, L2, S, L1HT, and SHT, where L stands for “large” (1086 atoms; cubic cell of edge 22.33 Å), S for “small” (362 atoms; 15.48 Å), and “HT” for high temperature. L1, L2, and S were run at room temperature, corresponding to several experiments, e.g. for the measurement

of the reaction rate of the CO₂ uptake;^{9,10} L1HT and SHT were equilibrated at a higher temperature (400 K), closer to solvent regeneration (see, e.g., ref 30). In the L1 samples, both zwitterion and carbamate conformers possess an internal hydrogen bond (HB), whereas this is not the case in the L2 and S samples. This choice allows us to sample different molecular configurations that are certainly present in real solutions. On the other hand, comparison of the L2 and S models helps understand and possibly rule out the effects of size on the results. All models contain CO₂ and MEA at concentrations of 9 and 30 wt %, respectively, and deuterated water.

In metadynamics, we used simple collective variables, namely, the N–H distance for deprotonation and the N–C distance for CO₂ release. In our work on diluted solution,¹⁹ we have validated this choice by comparing the MTD results to those of umbrella sampling. Moreover, MTD using the coordination number as collective variable gave the same results. In order to obtain an estimate of the enthalpy contribution to the free-energy barriers, we have calculated the Kohn–Sham (KS) energy for sets of configurations sampled in the domain of the reactant and in the region of the “transition state” (TS). The latter was refined with the use of the umbrella sampling technique.³¹ We also repeated the KS energy calculations within the B3LYP hybrid-functional scheme,²⁹ to obtain an estimate—although partial—of the dependence of our results on the choice of the exchange–correlation functional. These computations could be done in reasonable time only on the S and SHT samples, which are however shown to closely represent the larger systems. For a test of the procedures that we follow here, we refer to our simulations for dilute aqueous solutions in ref 19.

The (global) entropic component ($T\Delta S$) of the free-energy barrier for either CO₂ release or deprotonation can be estimated by subtracting the enthalpic barrier from the free-energy barrier. We also evaluated the specific contribution of the reacting molecule (carbamate or zwitterion), in the following way. First, in each trajectory of the reactant state (from equilibrium MD) or of the transition state, obtained from umbrella sampling, an alignment was made to eliminate rotations and translations. Then, a cluster analysis was performed employing the GROMOS algorithm³² with a fixed cutoff (maximum radius of the clusters), and the entropy difference was estimated as $\Delta S \approx k_B \log(N_{TS}/N_R)$ from the number of clusters in the reactant state N_R and in the transition state N_{TS} . The estimate turned out to be robust with respect to the cluster radius (see Table S2 in the SI).

We refer to the SI for more details.

2.2. Recall: More on the Simulations and System Setup of Previous Work. For the sake of comparison, here we report further details of the previous calculations by other authors, mentioned in the Introduction (with references taken from the original papers).

(a) In ref 12: The method combines Hartree–Fock geometry optimization with single-point calculations including the SM solvation model.³³

(b) In ref 15: All structures were optimized within the DFT-B3LYP functional and single-point G3MP2B3 calculations were performed to improve on the energy accuracy. The latter involve computations at the QCISD(T) level. Water is modeled with the polarizable-continuum-model (PCM).³⁴

(c) In ref 16: Both geometry optimizations and energy computations were carried out in the PCM with different choices of the cavity radii.

(d) In ref 17: In the scheme with molecular structures embedded in the continuum solvent model (PCM), DFT with the B3LYP functional is applied for geometry optimization, followed by single-point calculations at the couple-cluster (CCSD(T)) level. In the QM/MM approach, the classical force field is the TIP3P water model³⁵ and the DFT functional is B3LYP. Geometry optimizations are performed for the two subsystems separately: in the first step, the water molecules are kept fixed and the molecular structures of reactant and product complexes are relaxed, in the second step, the final geometries of the latter are kept fixed and the water configurations are optimized. Spherical boundary conditions are applied.

(e) In ref 18: DFT-MD with the PW91 functional model.³⁶ PBC are applied to a cubic unit cell of edge 8.639 Å containing 16 water molecules. The continuum solvation model is COSMO.³⁷

(f) In ref 20: DFT-MD with the PW91 functional.³⁶ PBC are applied to a cubic unit cell of edge 12.45 Å that contains one zwitterion and 59 water molecules.

3. RESULTS AND DISCUSSION

3.1. MEA Solution at Equilibrium. An example (L1) is illustrated in Figure 1, where one can see the formation of

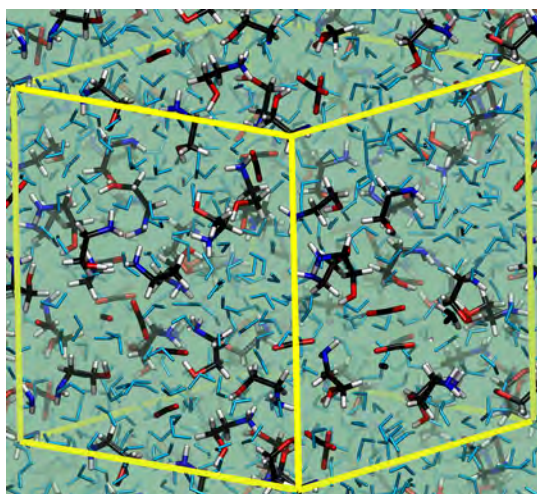


Figure 1. Snapshot of one of the samples used in our simulations (L1).

water-filled channels among the MEAs. Different isomers of the MEA molecules are present with predominance of gauche conformers.²⁴ Our systems at equilibrium were discussed in detail in ref 24. The results enabled us to interpret recent experimental data for both structural properties and vibrational spectra of MEA solutions with solvated CO₂ and after carbamate formation.

Further analysis is reported here. We especially searched for possible peculiar behavior of water in the solution and failed to find any sign of it.

First, one could wonder whether (confined) water or also MEA molecules form clusters. In our cluster analysis, we considered two water molecules to be in contact if the O–O distances was smaller than 3.5 Å, and two MEA molecules if any pair of respective atoms was closer than 3 Å to each other. According to this definition, we found that, throughout the

trajectory, all molecules of water formed a single cluster, i.e., they were not partitioned into multiple regions, and the same was true for MEA molecules.

Moreover, we evaluated the time-correlation function of the individual HBs as defined in ref 38. Comparison of (deuterated) water in the MEA solution with a bulk model (128 molecules) is reported in Figure 2a, where at variance with

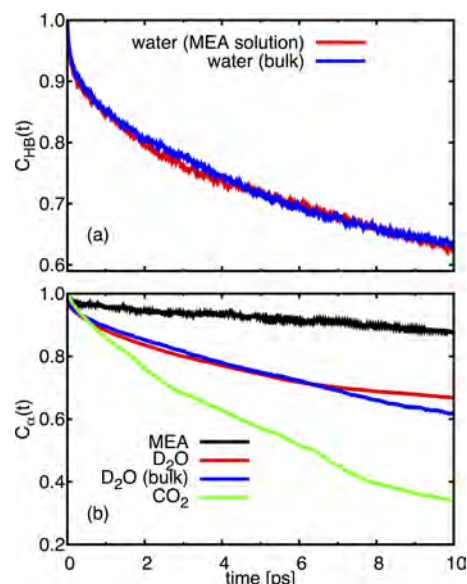


Figure 2. (a) Time-correlation function of the individual HBs. (b) Rotational correlation function for the orientation of MEA, water and CO₂ molecules in solution, and bulk water.

ref 38, normalization to unity is used for the sake of clarity. The correlation functions decay in an almost identical way, despite the different chemical environments in the two systems.

We computed the time correlation function of the orientation of MEA, water, and CO₂ molecules, according to the following formula:

$$C(t) = \frac{\langle \mathbf{n}(t_0) \cdot \mathbf{n}(t_0 + t) \rangle}{\langle \mathbf{n}^2 \rangle}$$

where \mathbf{n} is the unit vector associated with the orientation of a given molecule, e.g., directed along the C–C bond for MEA. The averages $\langle \dots \rangle$ are taken over all identical molecules, as well as over the initial time t_0 . The result is plotted in Figure 2b for the trajectory corresponding to the equilibrium dynamics of the zwitterion. The correlation function for the orientation of MEA molecules decays slowly, with a relaxation time of ~ 100 ps, namely one order of magnitude longer than for CO₂ and water. CO₂ is the fastest species due to the lack of strong directional bonds with the surrounding molecules. Water molecules rotate more quickly than MEA molecules due to the relatively rigid network of HBs and, as can also be seen in Figure 2b, exhibit the same behavior as in bulk water.

An insight into the electronic structure of the solution was also helpful to monitor the changes, namely, splittings and shifts of specific levels, along the reaction as discussed below. We calculated the Kohn–Sham electron states for several configurations at equilibrium. For a typical B3LYP density of states, we refer to Figure S1 in the SI. The width of the valence band, of which only 10 eV are covered in the plot, is ~ 27 eV.

The MEA gap is ~ 6 eV and the few midgap levels close to the LUMO are mostly localized on water molecules.

Structural characteristics of zwitterion and carbamate conformers in different samples of the solution are given and compared in Table S3 in the SI.

3.2. Reactions. According to experimental evidence, the overall reaction in eq 1, leading to the formation of carbamate and protonated amine, has an order equal to two and partial order in the amine equal to one. Consistency with the zwitterion mechanism in eqs 2, implies that deprotonation (eq 2b, forward) is faster than the reverse reaction regenerating the amine and solvated CO_2 (eq 2a, backward).

Here, we study both reactions in eqs 2a, representing the formation and dissociation of the zwitterion, deprotonation (eq 2b, forward) leading to the formation of the carbamate anion and its reverse (eq 2b, backward). No hydroxide ions are present in our systems. Quantitative results are given in Table 1, together with a sketch of the free-energy profile for the cyclic process.

MEA Zwitterion: CO_2 Capture and Release. Reaction rates measured with the stopped-flow technique over a temperature range of 298–313 K were fitted on the assumption of the zwitterion mechanism and provided an estimate of ~ 11 kcal/mol for the activation energy of the zwitterion formation.^{9,10} Our result (12 ± 3 kcal/mol) (Table 1) is in agreement with these data and indicate that, as expected,³⁹ entropic effects tend to contrast CO_2 uptake. We also find that the energy barrier is largely due to the breaking of hydrogen bonds involving the water molecules of the first solvation shell of CO_2 .

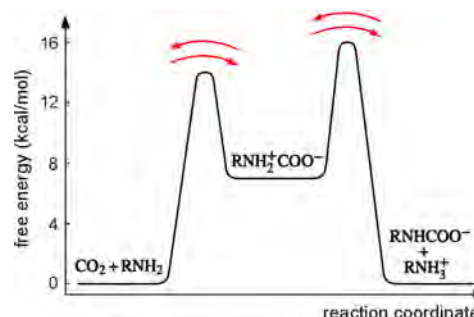
Snapshots from the simulations of these reactions are in Figure 3. The TS region (N–C in the range 2.3–2.5 Å) is more similar to the reactant domain than to the product (zwitterion): For example, the $\angle\text{OCO}$ bond angle is $165^\circ \pm 5^\circ$ and the number of the COO–water hydrogen bonds is only 0.5 ± 0.6 (see Table S4 in the SI), compared to $135^\circ \pm 4^\circ$ and 2.6 ± 0.5 , respectively, in the zwitterion; and the charge q at the carboxylate anion and the amine group (obtained from Mulliken population analysis) is small ($|q| < 0.1e$) in both cases, whereas it is approximately -0.4 and $+0.2$, respectively, in the zwitterion. This similarity also explains the strong difference (more than 10 kcal/mol) of the enthalpic barriers for CO_2 uptake and its reverse reaction (Table 1). From this comparison, one can also see that, contrary to the trend of the enthalpic barriers, the free-energy barrier for zwitterion formation is significantly higher than that for its dissociation. This difference implies that relative to MEA the zwitterion population is smaller by a factor 10^{-5} – 10^{-6} , which is consistent with the failure of experiments to detect it.

The direct participation of water in the process is responsible for the asymmetry of the reaction. Along the path from carboxylate anion to solvated CO_2 , while breaking the N–C bond with the amine, the COO moiety also loses hydrogen bonds (see Figure S2a in the SI) and the surrounding water molecules undergo a strong reorganization. Figure 4 illustrates the strong variation of the angles (axial (θ) and tilt (χ)) defining the orientation of water molecules, relative to CO_2 , from the reactant to the TS region, within a distance $\text{O}(\text{COO})\text{--O}_w$ of 3.5 Å. This important reorganization of the water network accompanying the release of CO_2 to the solvent, is consistent with the development of hydrophobic hydration of other small nonpolar solutes.⁴⁰ This scenario closely resembles our simulations of the same reaction in the 3 wt % solution,¹⁹ suggesting that the influence of MEA concentration is minor

Table 1. Free-Energy and Enthalpy Barriers for All Reactions Simulated Here (See Text) in 30 wt % MEA Aqueous Solutions^a

reaction	sample ^b	free energy, ΔF^* (kcal/mol) ^c	enthalpy, ΔE^* (kcal/mol) ^d
zwitterion formation	L2	15	
	S	14	12 [12]
CO_2 release from zwitterion	L1	10	
	L2	7	
	S	7	25 [24]
carbamate formation from zwitterion	L1	8	
	L2	9	
	S	9	12 [12]
CO_2 release from carbamate dissociation	L1	46	
	L1HT	51	
	L2	48	
	S	46	60 [62]
	SHT	49	62 [63]
MEA ⁺ deprotonation	L2	16	
	S	16	17 [18]

^aResults refer to BLYP-D2 values apart from those shown in square brackets, that have been obtained with the B3LYP functional on the same configurations of the BLYP-D2 simulations. ^bNote that L1, L2, and S refer to samples obtained at room temperature, whereas L1HT and SHT refer to samples obtained at 400 K. ^cErrors are estimated to be 2–3 kcal/mol. ^dErrors are estimated to be 3 kcal/mol.



and that the entropy change associated with the water rearrangement dominates the entropic component of the free-energy barriers. We can now justify this claim more precisely.

Indeed, a direct estimate of the entropy differences including all degrees of freedom of the solution, employing, e.g., the two-phase thermodynamic method,⁴¹ is not feasible due to the limited statistics available from our trajectories and to the presence of the harmonic restraint in the TS. However, we can evaluate the single contribution of the zwitterion, by using a structural cluster analysis³² to estimate the volume explored by the molecule in configuration space (see Table S2 in the SI for details). This approach does not require one to approximate the fluctuations with a set of oscillators⁴² and takes into account

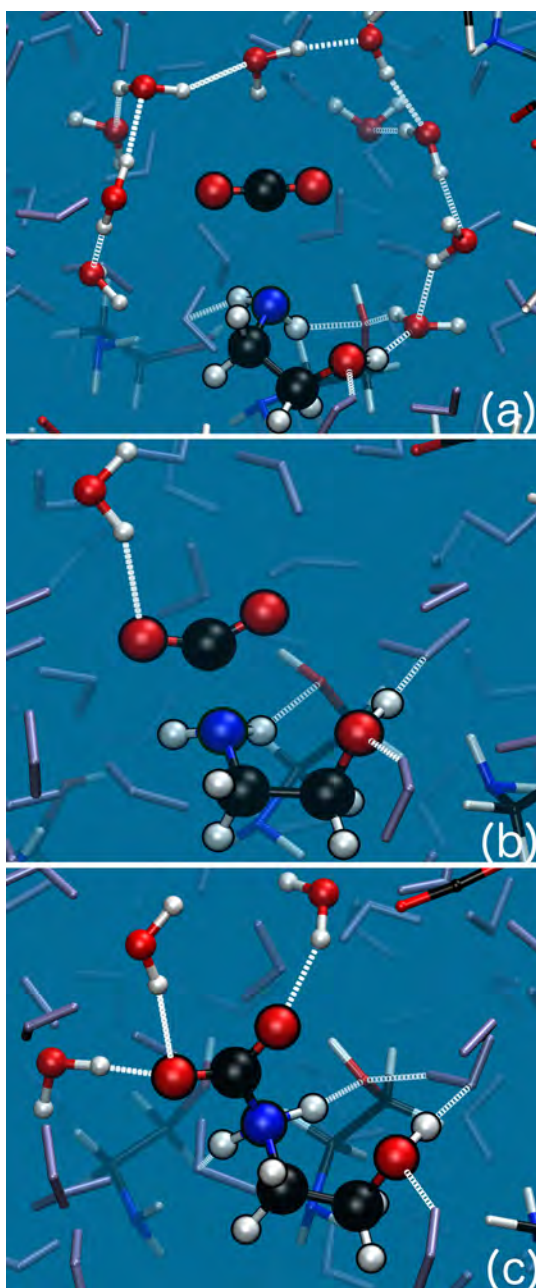


Figure 3. Zwitterion formation. Sketch of the reaction path in L2.

all anharmonic effects. The solute molecule turns out to contribute less than 1 kcal/mol to $T\Delta S$. We obtain the same result when we apply the same procedure to the trajectories of our simulations of the zwitterion in the dilute solution.¹⁹ The remainder is one order of magnitude larger and, therefore, must be associated with the degrees of freedom of the surrounding solution, and specifically to the water molecules, because the MEA molecules behave as orientationally frozen along the reaction, just as we have shown in the study of the equilibrium dynamics (see section 3.1).

The progression of the reactions is mirrored in the change of the density of KS states that are localized on the zwitterion. Figure 5a shows an example in the TS, namely, a particular state at ~ 2 eV below the highest occupied molecular orbital (HOMO), which is involved in the loss of the COO^- moiety. The disruption of the N–C bond pushes it up by ~ 1.5 eV.

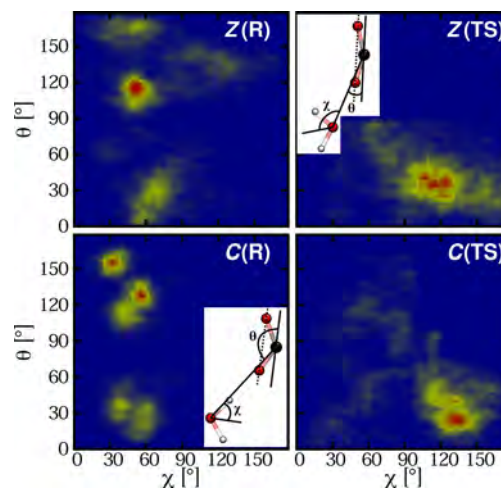


Figure 4. CO_2 release from the zwitterion (Z) and the carbamate (C). Variation of the angles depicted on the left, describing the reorientation of water molecules from the reactant (R) (panels on the left) to the TS (panels on the right).

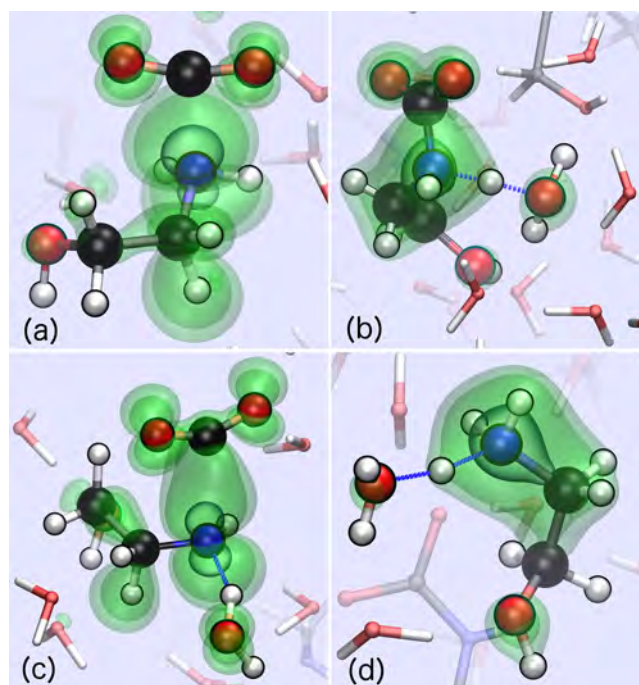


Figure 5. Probability density corresponding to one-electron states involved in (a) CO_2 release from the zwitterion, (b) zwitterion deprotonation, (c) CO_2 release from carbamate dissociation, and (d) MEAH^+ deprotonation (see text). Isosurfaces: 0.002, 0.005, 0.05 $e^-/(\text{a.u.})^3$.

We note that the free-energy barrier is higher in the L1 sample. This can be explained by the presence of an intra-hydrogen-bond peculiar to the zwitterion conformer in the L1 sample, which strengthens the binding of the carboxylate anion to the amine.

Formation of Carbamate Anion via Zwitterion Deprotonation. Any base present in the MEA solution, namely, either an amine or a water molecule or a hydroxide ion, can, in principle, drive deprotonation (eq 2b, forward). Our MTD simulations are unbiased, with respect to the reaction product: They start from a solution containing the zwitterion and use the N–H distance as the collective variable. At equilibrium, the

closer environment of the amine group of the zwitterion includes hydrogen-bonded molecules, either water or amines (via the hydroxyl group) (see Figure S3 in the SI). Different reaction paths are observed in the three different samples as shown in Figure 6. Water molecules always act as mediators of

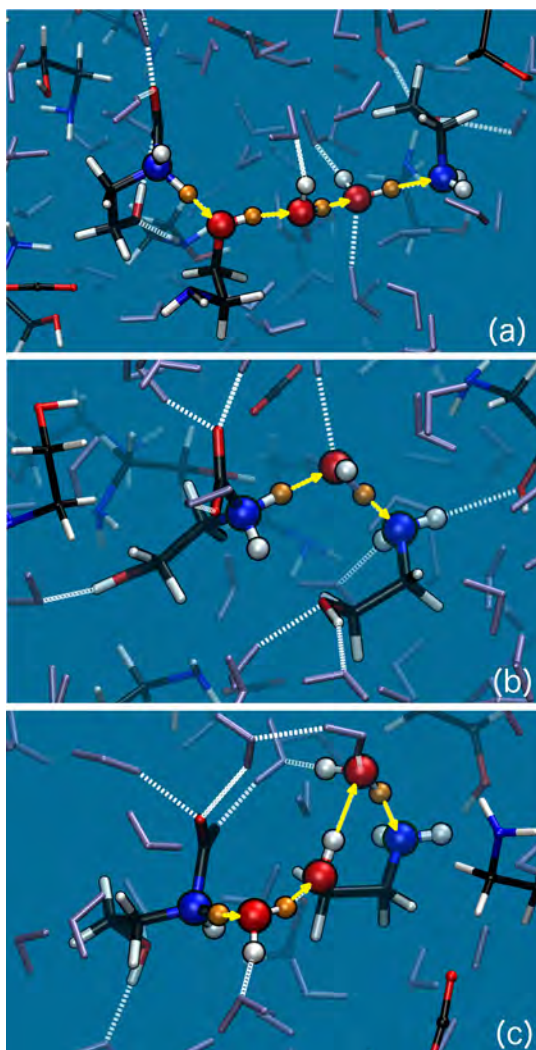


Figure 6. Zwitterion deprotonation. Sketch of the reaction path in three samples: (a) L1, (b) L2, and (c) S.

the reaction, which invariably ends in the formation of a protonated amine. However, in two out of three simulations, an unforeseen step is observed, namely, an amine participates in the formation of the proton chain, via its alcoholic termination (see Figures 6a and 6c).

Despite the different paths, not only the final proton transfer always ends into another amine, in agreement with eq 1 and the common knowledge that two amines are used for each CO₂ loaded (absorption capacity of MEA is 0.5 CO₂/mol amine), but the calculated free-energy barriers (ΔF^* , Table 1) are the same in the three samples within the accuracy of the calculations. This result is not surprising, because the barrier corresponds to the first step of the reaction chain and mainly depends on the strength of the hydrogen binding in the reactant. The following steps are barrierless. Two more comments are relevant here: (i) the value determined for ΔF^* is close to the value that we determined¹⁹ using similar

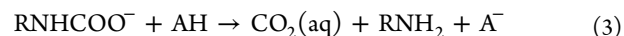
simulations for the proton transfer from the MEA-zwitterion to water in a dilute solution; and (ii) the entropic contribution, which we can deduce from Table 1, still facilitates the reaction but is not as relevant as for the dilute solution. Although the accuracy of this estimate is limited, the apparent reduction, with respect to the dilute solution, could result from the reduction of the water molecules available around the agent molecule. For example, in the L2(S) models, the latter shares 1.7 ± 0.6 (1.6 ± 0.6) HBs, whereas in the dilute solution, this number is 2.9 ± 0.7 . A slight reduction of the number of HBs (~ 0.5), a decrease of the HB length (from 1.84 Å to 1.64 Å) and especially a drastic reorientation of the nearby water molecules accompany the action of the mediating water. In analogy with the case of CO₂ release, the latter can be described by the variation of the axial (θ') and tilt (χ') angles. They respectively change from $80^\circ \pm 20^\circ$ to $147^\circ \pm 18^\circ$ and from $54^\circ \pm 15^\circ$ to $129^\circ \pm 20^\circ$. In the dilute solution, θ' varies from $88^\circ \pm 17^\circ$ to $152^\circ \pm 18^\circ$ and χ' varies from $55^\circ \pm 18^\circ$ to $122^\circ \pm 21^\circ$.

The effects of deprotonation on the electronic structure of the system can be singled out from the density of KS states: Figure 5b shows a particular state in a typical TS configuration. From a localized orbital on the amino group of the zwitterion—at ~ 18 eV below the HOMO—it deforms following the reaction and in the TS is shifted up by ~ 1 eV, relative to the reactant.

Contrary to the conclusions of ref 18, we do not find any evidence of direct proton transfer from the zwitterion to the amino group of a MEA. In order to check this issue further, we have performed a Gedanken experiment, namely, we have attempted to force such an event in two additional simulations, both starting from configurations having the convenient orientation and closeness of the zwitterion and a MEA molecule (see Figure 7a). However, they spontaneously moved away from each other and a water molecule entered between them (see Figure 7b). On the other hand, as shown above, in one case (sample S), we did observe direct (activated) transfer to the OH group of an amine, which is constantly hydrogen-bonded to water, and thus leads to a barrierless water protonation. Although not excluded, our simulations lead us to believe that direct zwitterion-amine transfer with formation of a protonated amine is improbable at a concentration of 30 wt %. From the brief account given in the Introduction and in section 2, one can argue that the predictions of ref 18 may suffer from severe limitations in the model size and in the configuration sampling (the reaction occurs within less than 1 ps of unbiased MD).

CO₂ Release from the Carbamate. Removal of CO₂ from the solution and recover of the amine is the most costly process in the case of MEA. Here, we focus on the early reaction step taking place in solution. Recent stopped-flow kinetic measurements on solutions at low concentration were interpreted in terms of a free-energy barrier of 15 kcal/mol for CO₂ release, with negligible entropic contribution (0.3 kcal/mol).³⁹

Carbamate Dissociation. The route commonly accepted for CO₂ release is the direct dissociation of the carbamate involving no intermediate:



where AH is any species that can act as an acid. AH is not necessarily the protonated amine of eq 1. Again, our MTD simulations, using the N–C distance as a collective variable, are not biased toward any specific proton donor or any specific product, other than a solvated CO₂. However, in our system,

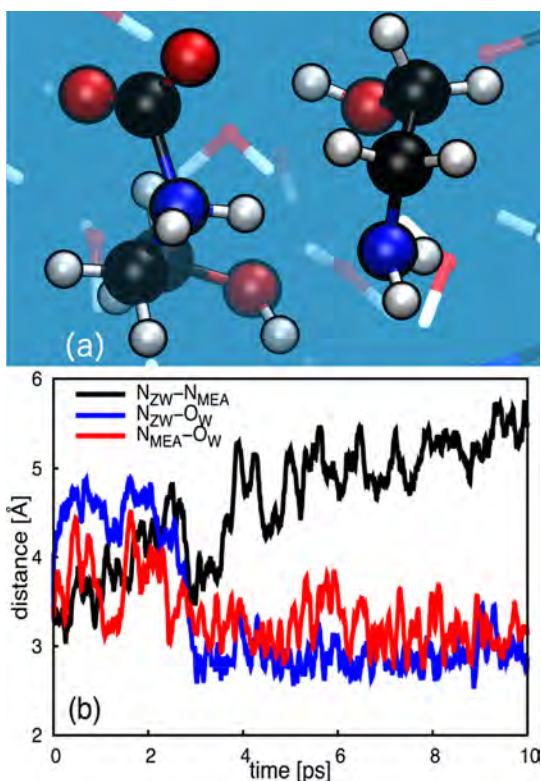


Figure 7. Gedanken experiment: (a) Simulations starting with the zwitterion and an amine at close distance and (b) variation of relevant distances with time. O_W denotes the oxygen of the water moving between the zwitterion and the amine.

only water molecules, surrounding the carbamate, act as acid. The protonated amine is also a candidate but, even if it happens to be close to the carbamate, the ultimate agent of proton transfer will invariably be a water molecule. Indeed, the NH_3^+ group is hydrogen-bonded to water (three HBs with a length of $1.8 \pm 0.1 \text{ \AA}$).

We have performed five simulations, three of which are at room temperature (for L1, L2, and S) and two are at 400 K (L1HT and SHT). The latter corresponds to typical conditions of the solvent regeneration process (see, e.g., ref 30). An example is illustrated in Figures 8a–c. In all our models, we observe the development of a concerted reaction, namely, the regeneration of the amine—via hydrogen abstraction from water—is concomitant to the loss of CO_2 from the carbamate. The coupling of these two processes can be appreciated in the distance evolution in Figure 9 and also in the spatial distribution of the HOMO of a typical configuration in the TS region (Figure 5c). Stronger changes in the electronic structure are observed than in the case of the release from the zwitterion, given the stronger binding of the CO_2 moiety. In particular, the formation of the characteristic electron state in Figure 5c induces a narrowing of the energy gap by $\sim 1 \text{ eV}$. As in the case of the zwitterion, the release of CO_2 is accompanied by a dramatic decrease of the hydrogen bonds (see Figure S2b in the SI) and a drastic reorientation of the surrounding water molecules (see Figure 4), leading to the “building up” of the hydrophobic cage.

The free-energy barrier—which is $\sim 50 \text{ kcal/mol}$ —is rather insensitive to the specific sample and moderately increases (by 3–4 kcal/mol) as the temperature increases from 300 K to 400 K. It is a factor of 5–7 times higher than in the case of release

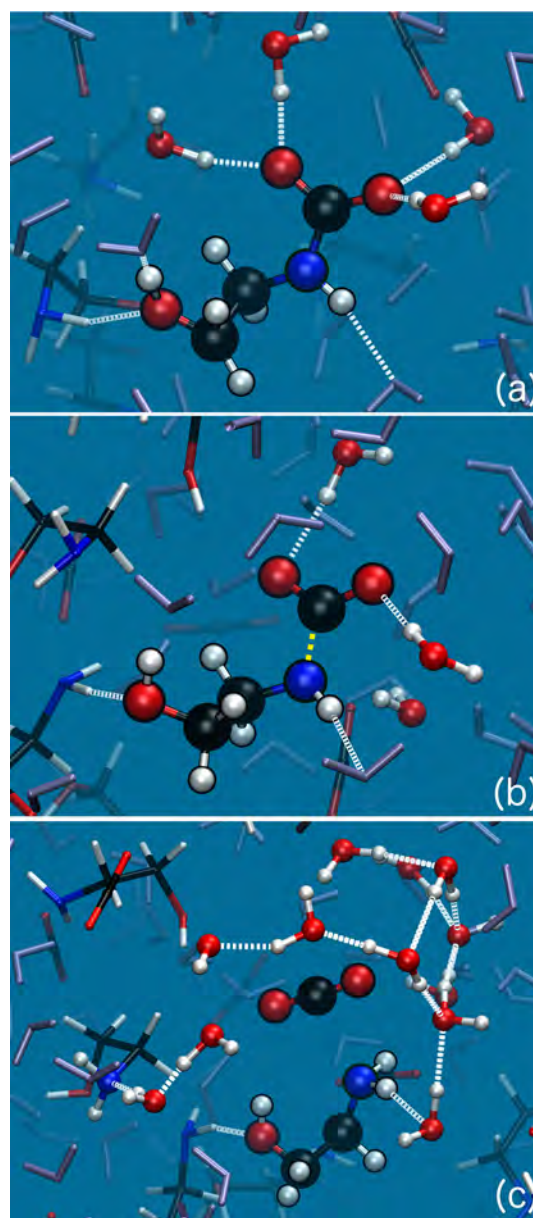


Figure 8. Carbamate dissociation. Sketch of the reaction path in L2: (a) reactant, (b) “transition state”, and (c) product.

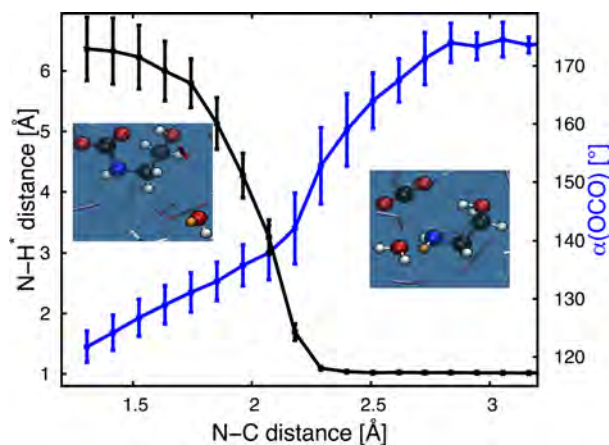


Figure 9. CO_2 release from the carbamate anion. Evolution of geometrical characteristics.

from the zwitterion. On one hand, the value of the enthalpic barrier (60 kcal/mol vs 25 kcal/mol) is much higher, which is consistent with the stronger bonding of the carboxylate anion in the carbamate—manifesting, e.g., in the shortening of the bond lengths (N–C bond and HBs, both internal and with water) (Table S3 in the SI)—and the product-like TS observed in all our MTD simulations (see Table S4 in the SI). On the other hand, the reorganization of the solvent facilitates the reaction via entropic effects but apparently to a lesser extent than in the case of the zwitterion.

Proton Release from a Protonated Amine. All our simulations of the direct release of CO₂ from carbamate clearly result in free-energy barriers that are too high. However, in principle, another path is possible, although never considered so far. This could again involve the zwitterion, through a two-step reaction: carbamate protonation at the nitrogen site (eq 2b, backward) and CO₂ release from the zwitterion (eq 2a, backward). As discussed above, the latter corresponds to a free-energy barrier of ~7–10 kcal/mol at room temperature. In analogy with the reaction leading to protonated amine formation (Figure 6), proton transfer from MEAH⁺ to the carbamate can occur via a proton wire. Our simulations confirm this scenario, involving an activated first step (deprotonation of MEAH⁺) followed by a sequence of barrierless events: diffusion of the hydronium in water and proton capture from the carbamate generating the zwitterion.

Figure 5d shows the distribution of a particular electron state that, in full analogy with the case of the zwitterion deprotonation, is involved in the reaction, namely from a localized orbital on the amino group, at ~19 eV below the HOMO, it evolves following the proton displacement. In the TS it is shifted upward by ~1 eV.

The rate-limiting step has a free-energy barrier of 16 kcal/mol with a negligible entropy contribution (see Table 1), in excellent agreement with the experiment.³⁹

We also remark that water splitting could be an additional proton source. However, further simulations indicate that this route implies a higher barrier and that the probable final product of water splitting in the close environment of the carbamate is not the zwitterion but carbamic acid, with a free-energy barrier of 20 kcal/mol.

4. CONCLUSIONS

The study that we have presented here for the chemical reactions, following the solvation of CO₂ molecules in MEA aqueous solutions, relies on large-scale simulations based on DFT molecular dynamics, aided by enhanced sampling techniques, as well as on an extensive analysis of the results. This approach has allowed us to search for the origin of the relevant barriers that the system must overcome, thus uncovering the microscopic mechanisms and quantitatively characterizing the entire cycle. Before drawing conclusions, we remark that, by summing up the barriers corresponding to all elementary reaction steps (see Table 1), we obtain an overall negligible free-energy difference between the CO₂ + MEA system and the carbamate + MEAH⁺ system. Within the precision of our simulations, this result is in agreement with the experiment³⁹ and thus demonstrates the global consistency of our calculations.

We propose a well-defined path that is consistent with the available experimental data. In this scenario, the carbamate-zwitterion RNH₂⁺COO⁻ plays a crucial role, being the ephemeral intermediate of both capture—in the form of

carbamate—and release reactions. In particular, zwitterion formation from solvated CO₂ and MEA turns out to be the rate-limiting step of the capture. Release does not follow the commonly assumed mechanism, namely, direct carbamate dissociation, but rather proceeds through an unforeseen two-step pathway: proton transfer from MEAH⁺ to the carbamate forming the zwitterion and its dissociation. Here, MEAH⁺ deprotonation is the rate-limiting step.

The role of water in the development of the reaction cycle is crucial, in determining both the paths and the energetics. Its amphoteric nature allows for the formation of a proton wire from one amine to another; as a proton acceptor, it can drive deprotonation, and, as a proton donor, it ensures amine regeneration. Moreover, water stabilizes the zwitterionic intermediate and facilitates CO₂ release from both the zwitterion and the carbamate via the entropy increase associated with the rearrangement of its structure. This effect is dramatic and, in particular, reverts the incorrect prediction of a higher population of the zwitterion, relative to CO₂ + MEA that one would infer from a mere calculation of enthalpic barriers.

Amine concentration affects the pathway leading to the formation of the carbamate, because different amines can intervene in the chain of proton transfer events. In contrast, along the CO₂ release pathway, the other amines behave as passive spectators.

The dynamics of chemical reactions in solution is a great challenge for chemical theory and simulations. Although not exhaustive, our set of simulations have provided important and unprecedented insights into the specific processes under study. Several remarks could be easily extended to other systems. In particular, we have observed that several different reactions can take place in the aqueous solution, leading to the same final products. Moreover, the presence of different conformers and, more generally, the heterogeneity of the solution suggests a distribution of free-energy barriers in the real system. This hints to caution in the comparison of single simulations and the experiment and may call for more-elaborate kinetic models for the derivation of reaction rates from observations.

■ ASSOCIATED CONTENT

Supporting Information

Computational details, molecular geometries calculated with different exchange-correlation functionals, more results of analysis of the simulations (as cited in the main text). The Supporting Information is available free of charge on the ACS Publications website at DOI: 10.1021/acs.jctc.5b00379.

■ AUTHOR INFORMATION

Corresponding Author

*E-mail: wanda.andreoni@epfl.ch.

Notes

The authors declare no competing financial interest.

■ ACKNOWLEDGMENTS

We acknowledge PRACE for awarding us access to the resource Juqueen, which is based in Germany at Jülich. Part of this work was supported as the CADMOS project and by the SNSF (under Project No. 132081). The financial support for CADMOS and for the Blue Gene/P system is provided by Geneva Canton, Vaud Canton, Foundation Hans Wilsdorf, Foundation Louis-Jeantet, the University of Geneva, the

University of Lausanne, and the Ecole Polytechnique Fédérale de Lausanne.

REFERENCES

- (1) Rochelle, G. T. *Science* **2009**, *325*, 1652–1654.
- (2) Wilcox, J. *Carbon Capture*; Springer: New York, 2012.
- (3) Isaacs, E.; Otto, F.; Mather, A. E. *J. Chem. Eng. Data* **1980**, *25*, 118–120.
- (4) Kittel, J.; Idem, R.; Gelowitz, D.; Tontiwachwuthikul, P.; Parrain, G.; Bonneau, A. *Energy Procedia* **2009**, *1*, 791–797.
- (5) Abu-Zahra, M. R. M.; Niederer, J. P. M.; Feron, P. H. M.; Versteeg, G. F. *Int. J. Greenhouse Gas Control* **2007**, *1*, 135–142.
- (6) (a) Puxty, G.; Rowland, R.; Allport, A.; Yang, Q.; Bown, M.; Burns, R.; Maeder, M.; Attalla, M. *Environ. Sci. Technol.* **2009**, *43*, 6427–6433; (b) Porcheron, F.; Gibert, A.; Mougin, F.; Wender, A. *Environ. Sci. Technol.* **2011**, *45*, 2486–2492.
- (7) Caplow, M. *J. Am. Chem. Soc.* **1968**, *90*, 6795–6803.
- (8) (a) Danckwerts, P. V. *Chem. Eng. Sci.* **1979**, *34*, 443–446; (b) Blauwhoff, P.; Versteeg, G. F.; van Swaaij, W. P. M. *Chem. Eng. Sci.* **1984**, *39*, 207–225; (c) Versteeg, G. F.; van Swaaij, W. P. M. *Chem. Eng. Sci.* **1988**, *43*, 573–585.
- (9) Alper, E. *Ind. Eng. Chem. Res.* **1990**, *29*, 1725–1728.
- (10) Ali, S. *Int. J. Chem. Kinet.* **2005**, *37*, 391–405.
- (11) (a) Mani, F.; Peruzzini, M.; Stoppioni, P. *Green Chem.* **2009**, *8*, 995–1000; (b) McCann, N.; Phan, D.; Wang, X.; Conway, W.; Burns, R.; Attalla, M.; Puxty, G.; Maeder, M. *J. Phys. Chem. A* **2009**, *113*, 5022–5029.
- (12) da Silva, E. F.; Svendsen, H. F. *Ind. Eng. Chem. Res.* **2004**, *43*, 3413–3418.
- (13) da Silva, E. F.; Svendsen, H. F. *Ind. Eng. Chem. Res.* **2006**, *45*, 2497–2504.
- (14) da Silva, E. F.; Kuznetsova, T.; Kvamme, B.; Merz, K. M. *J. Phys. Chem. B* **2007**, *111*, 3695–3703.
- (15) Arstad, B.; Blom, B.; Swang, O. *J. Phys. Chem. A* **2007**, *111*, 1222–1228.
- (16) Shim, J. G.; Kim, J. H.; Jhon, Y. H.; Kim, J.; Cho, K. H. *Ind. Eng. Chem. Res.* **2009**, *48*, 2172–2178.
- (17) Xie, H.; Zhou, Y.; Zhang, Y.; Johnson, J. K. *J. Phys. Chem. A* **2010**, *114*, 11844–11852.
- (18) Han, B.; Zhou, C.; Wu, J.; Tempel, J. T.; Cheng, H. *J. Phys. Chem. Lett.* **2011**, *2*, 522–526.
- (19) Guido, C. A.; Pietrucci, F.; Gallet, G. A.; Andreoni, W. *J. Chem. Theory Comput.* **2013**, *9*, 28–32.
- (20) Sumon, K.; Henni, A.; East, A. *J. Phys. Chem. Lett.* **2014**, *5*, 1151–1156.
- (21) da Silva, E. F.; Svendsen, H. F. *Int. J. Greenhouse Gas Control* **2007**, *1*, 151–157.
- (22) Car, R.; Parrinello, M. *Phys. Rev. Lett.* **1985**, *55*, 2471–2474.
- (23) (a) Laio, A.; Parrinello, M. *Proc. Natl. Acad. Sci. U.S.A.* **2002**, *99*, 12562–12566; (b) Barducci, A.; Bonomi, M.; Parrinello, M. *Comput. Mol. Sci.* **2011**, *1*, 826–843.
- (24) Ma, C.; Pietrucci, F.; Andreoni, W. *J. Phys. Chem. Lett.* **2014**, *5*, 1672–1677.
- (25) (a) Becke, A. D. *Phys. Rev. A* **1988**, *38*, 3098–3100; (b) Lee, C.; Yang, W.; Parr, R. G. *Phys. Rev. B* **1988**, *37*, 785–789; (c) Grimme, S. *J. Comput. Chem.* **2006**, *27*, 1787–1799.
- (26) Troullier, N.; Martins, J. L. *Phys. Rev. B* **1991**, *43*, 1993–2006.
- (27) CPMD, Copyright IBM Corp. (1990–2014), and MPI für Festkörperforschung Stuttgart (1997–2001).
- (28) (a) Perdew, J. P.; Burke, K.; Ernzerhof, M. *Phys. Rev. Lett.* **1996**, *77*, 3865–3868; (b) Perdew, J. P.; Burke, K.; Ernzerhof, M. *Phys. Rev. Lett.* **1998**, *80*, 891–894.
- (29) (a) Stephens, P. J.; Devlin, F. J.; Chabalowski, C. F.; Frisch, M. J. *J. Phys. Chem.* **1994**, *98*, 11623–11627; (b) Vosko, S. H.; Wilk, L.; Nusair, M. *Can. J. Phys.* **1980**, *58*, 1200–1211.
- (30) Choi, W.-J.; Seo, J.-B.; Jang, S.-Y.; Jung, J.-H.; Oh, K.-J. *J. Environ. Sci.* **2009**, *21*, 907–913.
- (31) Torrie, G. M.; Valleau, J. P. *J. Comput. Phys.* **1977**, *23*, 187–199.
- (32) Daura, X.; Gademann, K.; Jaun, B.; Seebach, D.; van Gunsteren, W. F.; Mark, A. E. *Angew. Chem., Int. Ed.* **1999**, *38*, 236–240.
- (33) Chambers, C. C.; Hawkins, G. D.; Cramer, C. J.; Truhlar, D. G. *J. Phys. Chem.* **1996**, *100*, 16385–16398.
- (34) (a) Mieltus, S.; Scrocco, E.; Tomasi, J. *Chem. Phys.* **1981**, *55*, 117–129; (b) Cossi, M.; Scalmani, G.; Rega, N.; Barone, V. *J. Chem. Phys.* **2002**, *117*, 43–55.
- (35) Jorgensen, W. L.; Chandrasekhar, J.; Madura, J. D.; Impey, R. W.; Klein, M. *J. Phys. Chem. B* **1983**, *79*, 926–935.
- (36) Perdew, J. P.; Chevary, J. A.; Vosko, S. H.; Jackson, K. A.; Pederson, M. R.; Singh, D. J.; Fiolhais, C. *Phys. Rev. B* **1991**, *46*, 6671–6687.
- (37) Klamt, A.; Schurmann, G. *J. Am. Chem. Soc.* **1993**, *2*, 799–805.
- (38) Raiteri, P.; Laio, A.; Parrinello, M. *Phys. Rev. Lett.* **2004**, *93*, 087801–087804.
- (39) Conway, W.; Wang, X.; Fernandes, D.; Burns, R.; Lawrance, G.; Puxty, G.; Maeder, M. *J. Phys. Chem. A* **2011**, *115*, 14340–14349.
- (40) (a) Grossman, J. C.; Schwegler, E.; Galli, G. *J. Phys. Chem. B* **2004**, *108*, 15865–15872; (b) Allesch, M.; Schwegler, E.; Galli, G. *J. Phys. Chem. B* **2007**, *111*, 1081–1089.
- (41) Lin, S.-T.; Maiti, P. K.; Goddard, W. A., III. *J. Phys. Chem. B* **2010**, *114*, 8191–8198.
- (42) Karplus, M.; Kushick, J. *Macromolecules* **1981**, *14*, 325–332.